Research Article GU J Sci 32(2): 544-556 (2019)

Gazi University

**Journal of Science**

http://dergipark.gov.tr/gujs

# High Efficiency Axial Flux Permanent Magnet Machine Design for Electric Vehicles

Naghi ROSTAMI[1,*]

[1]*Faculty of Electrical and Computer Engineering, University of Tabriz, Tabriz, Iran*

**Article Info**

*Received: 18/04/2018*
*Accepted: 10/11/2018*

**Keywords**

*Electric vehicle*
*Axial-Flux Permanent-Magnet machines*
*Traction motor*
*Design optimization*

**Abstract**

Design and optimization of electrical machines for electric vehicle (EV) applications is a challenging task. In response to variable driving circumstances, the machine should be designed to operate in a wide range of speed and torque. This paper aims to optimize a surface-mounted axial-flux permanent-magnet (AFPM) traction machine taking the influence of the driving cycle into account. The AFPM motor is designed to maximize the overall efficiency over a predefined driving cycle. EV requirements and geometric constraints are taken into account in the design process. Hundreds of operating points in a driving cycle are reduced to the limited number of representative points by calculating the energy centre points in the energy distribution curve. Therefore, the number of calculations during the design optimization is significantly reduced. An analytical design procedure based on quasi-3D approach is used for accurate modelling of AFPM machine and genetic algorithm (GA) is implemented to find out the optimal design parameters. Functionality of the proposed approach is validated via comprehensive three-dimensional (3D) finite-element analysis (FEA).

## 1. INTRODUCTION

With the increased concerns about environmental problems, electric vehicles (EVs) seem to have a major role in the future transportation systems [1]. To improve the overall performance of the EV, an appropriate electrical machine should be selected and optimized to satisfy the design requirements. The power density and efficiency are the most important attributes for traction applications. Permanent magnet (PM) machines are usually preferred among other types of electrical machines such as induction machine (IM) and switched reluctance machine (SRM) [2–6]. Even though, IMs can be operated in a wide range of speed and torque, they have a lower torque density, lower efficiency, and lower power factor compared to PM machines. Similarly, SRMs have a higher torque ripple and a poorer power factor [7,8]. It must be noted that, the PM machine has own drawbacks, such as expensive PM materials, low speed ratio between the maximum and rated speed, and relatively low efficiency at field weakening region due to demagnetizing current.

Owing to the high torque density, modular and compact construction, high efficiency over wide speed-torque range and easy integration with other mechanical components, axial flux permanent magnet (AFPM) machines seem to be a competitive or even a better choice for EV applications [9–15]. Furthermore, low axial length of AFPM machines makes it possible to use them in particular applications such as in-wheel traction motors [9]. Authors in [16] have compared axial flux and radial flux machines for the use in wheel hub drives in terms of their power densities. In [17], the dimensions of an AFPM coreless machine have been optimized to achieve the highest power density. However, the machine was optimized for only one working point. Darabi *et al.* in [18] have presented an analytical design tool to optimize a double-sided AFPM motor. The machine design algorithm receives the machine rated parameters and design constraints and yields the optimal design parameters. Authors in [19] have evaluated the use of an AFPM in-wheel motor for an electric bicycle.

*Corresponding author, e-mail: n-rostami@tabrizu.ac.ir

Traction motors are traditionally designed to meet the basic requirements of rated or maximum power, torque, and speed. Even though, these specifications provide a baseline for machine designers, the design parameters may not be sufficiently reliable in practice [20]. In [21], the influence of the different driving conditions on the traction motor performance has been demonstrated. It has been shown that, the machine design parameters optimized for different driving cycles would be quite different. In [22], driving condition has been taken into account in the design process of a radial-flux permanent-magnet (RFPM) Machine for EV applications. However, the machine efficiency was not optimized.

The EV traction machines should be able to operate over a wide range of torque-speed. At low speeds or standstill, they have to produce high torque to accelerate the vehicle. Furthermore, the machine should provide high output power, usually 2 times of nominal value, at medium to high speed [23]. Since the working points of a traction motor vary in response to variable driving conditions, an appropriate design technique should be used to improve the traction machine overall efficiency not only, around the rated operating point [24] or a few points around the rated point [25] but over the whole predefined driving cycle.

The problem, however is that regarding the large number of operating points in a driving cycle, the design and optimization process may be very time consuming or even infeasible. In this paper, an efficient design optimization approach based on driving cycle representative point technique [26] has been presented. Quasi-3D approach is used for accurate modelling of AFPM machine and genetic algorithm (GA) is used as an optimization tool. Furthermore, comprehensive FEA is carried out to verify the obtained results.

## 2. ENERGY DISTRIBUTION OVER A DRIVING CYCLE

### 2.1. Considered Driving Cycle

New European drive cycle (NEDC) has been widely used to evaluate the energy consumption and the emission level of the vehicles, especially in Europe. It is composed of four urban driving cycles called ECE 15 followed by one extra urban driving cycle (EUDC). The ECE 15 is specified by low speed and low engine demand representing city driving conditions while EUDC includes more demanding, aggressive, and high speed driving pattern [27]. The main specifications of the considered driving cycles are listed in Table 1.

***Table 1.*** *Main parameters of the considered driving cycles [27]*

| Characteristics | ECE 15 | EUDC |
|---|---|---|
| Distance (km) | 4×1.013=4.052 | 6.955 |
| Duration (sec) | 4×195=780 | 400 |
| Mean speed (km/h) | 18.7 (with idling) | 62.6 |
| Maximum speed (km/h) | 50 | 120 |

### 2.2. Vehicle Characteristics and Energy Distribution over NEDC

To obtain the motor operating range of speed and torque over a predefined driving cycle, the vehicle components, road and driver models have been implemented in Simulink/Matlab. Modelling of EV is not the key concern in this paper and only design improvement of electrical machine used in EV has been considered. The detail on how to model the EV components such as the driver, road, electric machine, transmission, and battery can be found in [1]. The main data of the considered vehicle are listed in Table 2.

***Table 2.*** *Considered vehicle data*

| Parameter | Value |
|---|---|
| Wheel radius (m) | 0.3 |
| Vehicle weight (kg) | 1600 |
| Rolling resistance | 0.008 |
| Drag coefficient | 0.26 |
| Front area ($m^2$) | 2.55 |
| Auxiliary power (kW) | 1 |
| Air density ($kg/m^3$) | 1.2 |
| Gear ratio for the gear between the wheels and traction motor | 3.51 |
| Efficiency of differential | 0.98 |
| Gravitational acceleration ($m/s^2$) | 9.81 |

The motor speed and torque profiles and the resultant power characteristics of the vehicle over the predefined cycle are given in Figure 1. The large number of working points in the time domain is clear which should be reduced into a reduced number of representative torque-speed points by calculating the energy centre points.

It must be noted that the various driving condition and driver's habits in the acceleration and braking period may significantly influence the efficiency of the vehicle components and energy consumption level.

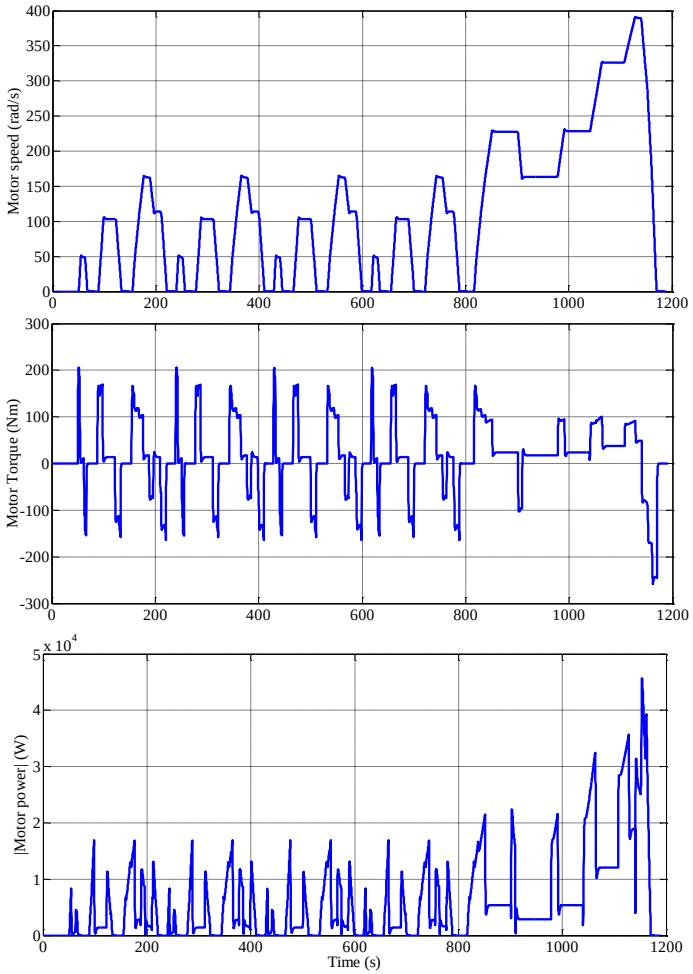


***Figure 1.*** *Traction motor characteristics over the NEDC*

If constant speed $\omega_m(t_i)$ and torque $T_m(t_i)$ is assumed along the time duration $\Delta t_i$, the power $P_m(t_i)$ and energy use $E_{t_i}$ at each time $t = t_i$ can be defined as

$$P_m(t_i) = T_m(t_i) \times \omega_m(t_i) \tag{1}$$

$$E_{t_i} = P_m(t_i) \times \Delta t_i \tag{2}$$

The energy consumption versus motor speed and output torque is illustrated in Figure 2. As it is obvious, there are six operational points with significantly higher energy consumption compared to others. These points are related to the constant speed with relatively low torque periods in the NEDC. Therefore, these points have major importance on the motor efficiency. Other widely scattered points with the relatively low energy consumption can be represented as the groups of working points based on the energy "centre of gravity" of the energy distribution pattern after removing the first 6 points. Six sub-regions, listed in Table 3, are considered according to Figure 3.

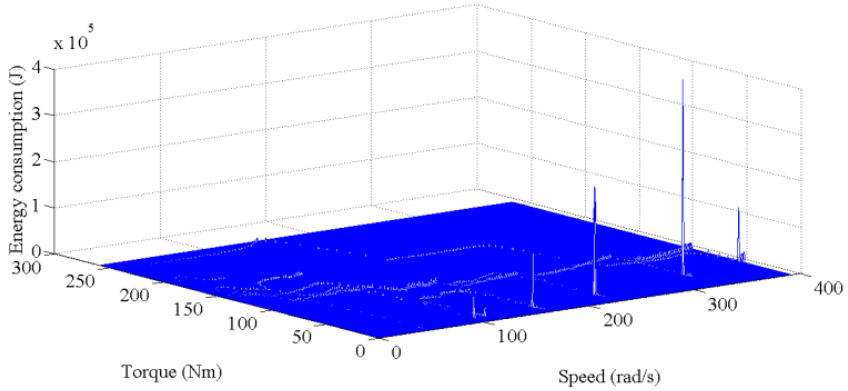


***Figure 2.*** *Energy distribution of the traction motor working points*

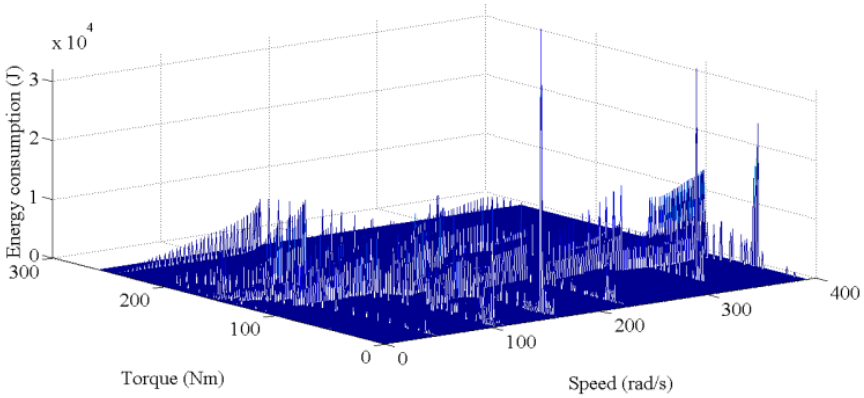


***Figure 3.*** *Energy distribution of the traction motor working points after removing 6 high energy points*

***Table 3.*** *Considered sub-regions for widely scattered operational points with relatively low energy distribution*

| Region number | $T_m$(Nm) | $\omega_m$(rad/sec) |
|---|---|---|
| Region 1 | 200 – 258 | 0 – 200 |
| Region 2 | 120 – 200 | 0 – 150 |
| Region 3 | 100 – 200 | 150 – 390 |
| Region 4 | 0 – 120 | 0 – 150 |
| Region 5 | 0 – 100 | 150 – 300 |
| Region 6 | 0 – 150 | 300 – 390 |

The energy distribution at region $i$ is centred at the corresponding representative point ($T_{mci}$, $\omega_{mci}$) and can be obtained as

$$T_{mci} = \frac{1}{E_i} \sum_{j=1}^{N_i} E_{ij} T_{ij} \tag{3}$$

$$\omega_{mci} = \frac{1}{E_i} \sum_{j=1}^{N_i} E_{ij} \omega_{ij} \tag{4}$$

where $N_i$ is the working points number at region $i$ and $E_i$ is the sum of energy at region $i$ and can be defined as

$$E_i = \sum_{j=1}^{N_i} E_{ij} \tag{5}$$

Twelve representative points over the NEDC are listed in Table 4. The first six points are those with significantly high level of energy consumption as illustrated previously in Figure 2. The next six points are the representative points for the considered sub-regions. The trajectory of operational points over NEDC and the selected representative points for the traction machine is shown in Figure 4. It is obvious that, thousands of operating points in the specific driving cycle are reduced to twelve representative points which consequently results in the reduced computational time while maintaining fair accuracy.

***Table 4.*** *Twelve representative points over the NEDC*

| Speed (rad/s) | Torque (Nm) | Energy (kJ) | Normalized (%) |
|---|---|---|---|
| 325.78 | 37.12 | 423.2 | 6.06 |
| 227.85 | 23.64 | 234.6 | 3.36 |
| 248.67 | 23.734 | 227.7 | 3.26 |
| 163.28 | 17.36 | 176.7 | 2.53 |
| 389.89 | 48.52 | 117.3 | 1.68 |
| 103.32 | 13.39 | 89.4 | 1.28 |
| 113.55 | 239.5 | 226.3 | 3.24 |
| 60.07 | 149.41 | 852 | 12.2 |
| 216 | 139.6 | 554.5 | 7.94 |
| 106.45 | 92.46 | 1445.5 | 20.7 |
| 214.72 | 77.39 | 1319.8 | 18.9 |
| 350.38 | 79.54 | 1316.3 | 18.85 |

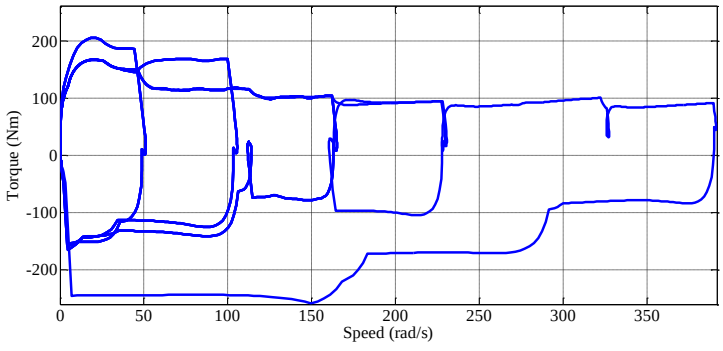


*(a)*

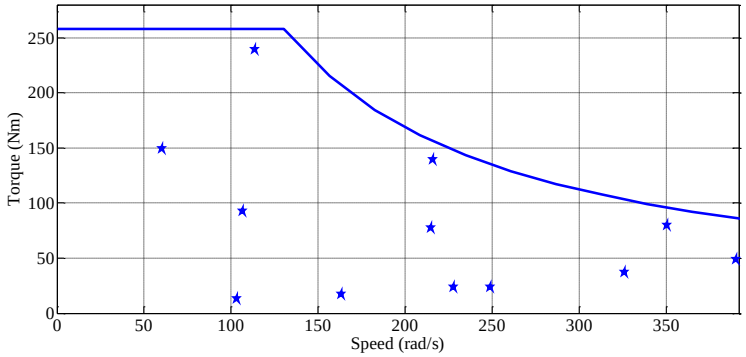


*(b)*

***Figure 4.*** *Characteristics of electrical machine over considered cycle; a) Torque-speed trajectory over NEDC b) The selected representative points under the motor operating point's envelope*

### 2.3. Validation of Representative Points

To assess the validity of the selected representative points, the total loss of energy for the traction motor is respectively calculated along all points of the NEDC and over 12 representative points according to equations (6) and (7).

$$EL = \sum_{i=1}^{N} T_m(t_i)\omega_m(t_i)\Delta t_i\,(1-\eta_i)/\eta_i \tag{6}$$

$$EL = \sum_{j=1}^{12} E_j\,(1-\eta_j)/\eta_j \tag{7}$$

where $\eta_i$ is the considered machine efficiency at $\omega_m(t_i)$ and $T_m(t_i)$. $E_j$ and $\eta_j$ is the energy consumption and efficiency, at the $j^{th}$ point, respectively.

The main specifications of the selected motor are listed in Table 5. Comparison of the results is given in Table 6. It can be concluded that, the representative points are a good representative of all traction motor operational points.

***Table 5.*** *The main machine design specifications*

| | |
|---|---|
| Rated speed (rad/s) | 130 |
| Maximum speed (rad/s) | 390 |
| Rated torque at constant torque region (Nm) | 258 |
| Maximum current density ($A/mm^2$) | 10 |
| Acceptable maximum line voltage ($V_{rms}$) | 250 |

***Table 6.*** *Comparison of energy losses over all points and the selected 12 representative points*

| | |
|---|---|
| Sum of energy loss for all working points (kJ) | 396.2 |
| Sum of energy loss for selected 12 representative points (kJ) | 381.71 |
| Difference (%) | 3.65 % |

## 3. DESIGN APPROACH

### 3.1. Reference AFPM Machine and Quasi-3D Computation Design Program

As illustrated in Figure 5, an Interior rotor double-sided AFPM machine with twelve Neodymium Iron-Boron magnet poles on each side of the rotor is considered as a reference machine. Two stators consist 36-rectangular slots comprising a two layer lap winding.

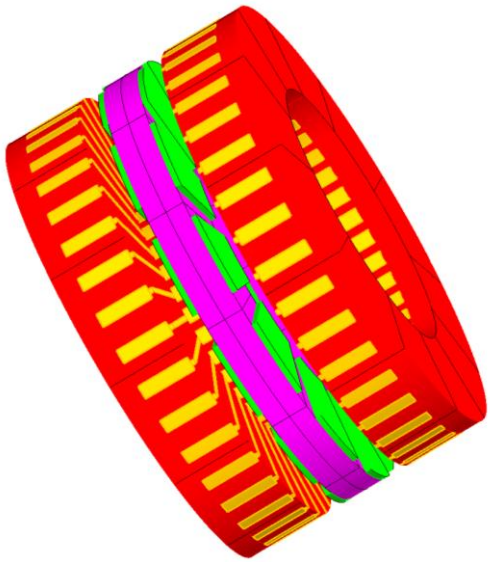

***Figure 5.*** *The reference AFPM machine*

To achieve sufficiently accurate computation results, the intrinsic 3D structure of AFPM machines should be taken into account. In this paper, quasi-3D approach is applied to perform a 3D design calculation by subdividing the machine structure into sufficient number of independent 2D planes and obtaining the machine overall performance by summing the computed results for each plane [10].

A design program using the basic equations needed for AFPM machine design [11] and quasi-3D approach, is utilized. GA is used to find out the most appropriate design parameters over NEDC. The details of the quasi-3D approach, design procedure, and GA implementation are not the key concerns in this paper and can be found in other papers published by author *et al.* [12-14].

### 3.2. Optimization Parameters, Objective and Constraints

As expressed in equation (8), the optimization process tends to minimize the sum of the energy loss in the computed representative points.

$$W_{loss} = \sum_{i=1}^{m} P_{loss}(T_{mci}, \omega_{mci})\Delta t_{mi} \tag{8}$$

where $m$ is the number of selected representative points, $P_{loss}(T_{mci}, \omega_{mci})$ is the power loss at $i^{th}$ representative point, and $\Delta t_{mi}$ is the total time interval of the $i^{th}$ representative point.

Stator outer diameter, the inner to outer diameter ratio, the relative magnet width, and flux density in the air-gap region are the main design parameters to be optimized.

Electromagnetic design consideration, practical and mechanical restrictions are regarded in the design process [12]. Several machine design constraints are given in Table 7.

***Table 7.*** *Several machine design constraints*

| Parameter | Value |
|---|---|
| Stator core outer diameter, $D_{out}$ (mm) | $300 \le D_{out} \le 400$ |
| Diameter ratio, $K_D$ | $0.57 \le K_D \le 0.65$ |
| Flux density at the air gap region, $B_{agap}$ (T) | $0.75 \le B_{agap} \le 0.85$ |
| Relative magnet width, $\alpha_p$ | $0.6 \le \alpha_p \le 0.85$ |
| Minimum teeth thickness (mm) | $\ge 5$ |
| Line-to line induced back-EMF (V) | $\le 250$ |
| Maximum current density ($A/mm^2$) | 10 |
| Machine axial length (mm) | $\le 120$ |

### 3.3. Design Optimization

As observed in Figure 2, the majority of points with relatively high energy consumption are placed in the low-torque zone. Therefore, the optimum operation over all points of the driving cycle would not be achieved by optimizing the traction machine against the nominal power point.

The difference between the design optimization results at the nominal operating point and over the predefined cycle is demonstrated in this section. The main design parameters of two optimized machines are listed in Table 8. The first machine which is denoted by "Design A" is optimized over NEDC while the second machine which is denoted as "Design B" is optimized at rated operating point. The same set of constrains are defined for both designs.

***Table 8.*** *Optimized AFPM machine data*

| Parameter | Design A | Design B |
|---|---|---|
| Pole pairs, $p$ | 6 | |
| Stator slots, $Q_s$ | 36 | |
| Air-gap thickness, $g$ (mm) | 1.5 | |
| Magnet material | Nd-Fe-B | |
| Stator outer diameter, $D_{out}$ (mm) | 301.1 | 364.4 |
| Diameter ratio, $K_D$ | 0.6496 | 0.5712 |
| Machine axial length (mm) | 99.8 | 101.2 |
| Relative magnet width, $\alpha_p$ | 0.7 | 0.68 |
| PM height, $h_{PM}$ (mm) | 4 | 6.8 |
| Stator yoke height, $h_y$ (mm) | 11.4 | 14.9 |
| Teeth height, $h_{ds}$ (mm) | 17.2 | 8.9 |
| Rotor disk height, $h_{yr}$ (mm) | 25.6 | 31 |
| Width of the rectangular slots, (mm) | 9.4 | 10 |
| Coil turns per phase | 48 | 24 |

| | | |
|---|---|---|
| Phase resistance at $120\,^{\circ}C$ $(m\Omega)$ | 52.5 | 27.3 |
| Current density at rated point $(A/mm^2)$ | 6.63 | 6 |

### 3.4. Discussion on the Results

To compare two optimized machines, the main power loss components of both machines are calculated. Copper and iron losses of the machines as well as their corresponding efficiencies at the rated power points are listed in Table 9.

***Table 9.*** *Major power loss component and efficiency comparison for two designs at rated point*

| Parameter | Design A | Design B |
|---|---|---|
| Copper loss at rated point $(W)$ | 1082.6 | 604.25 |
| Iron loss at rated point $(W)$ | 196.37 | 347.49 |
| Efficiency at rated point $(\%)$ | 95.35 | 96.16 |

As it is clear, "Design B", which is optimized at rated point, presents a higher efficiency at rated operating point compared to "Design A". The reason is that, the main objective of "Design B" is to minimize the copper loss in the winding which is the dominant part of the machine losses. According to Table 8, this can be realized by increasing the slot width. The saturation level at the stator teeth must be kept at an acceptable value. Therefore, smaller phase resistance, lower current density and consequently, lower copper loss is achieved in "Design B". Furthermore, "Design B" has less turns per phase leading to a lower copper loss. On the other hand, "Design B" presents a higher iron loss due to the higher magnetic saturation levels and larger axial length. However, once two optimized machines are evaluated over 12 representative points, different results are observed. The overall efficiency and the total values of the loss components are given in Table 10 for both designs. This difference is mainly due to the fact that, the highest energy consumption occurs at low-torque high-speed points. In these points the iron loss becomes the most dominating part of the losses. Therefore, "Design B" with relative high iron loss component would not be an optimal solution over the driving cycle. In contrast to "Design B", lower iron loss is realized in "Design A". This is due to lower saturation levels in the stator teeth and shorter axial length of the machine. Furthermore, shorter axial length leads to a lighter machine with lower cost. It can be concluded that, with an appropriate optimization strategy, higher efficiency at a predefined driving cycle can be obtained even with lower cost.

***Table 10.*** *Major power loss component and efficiency comparison for two designs over 12 representative points*

| Parameter | Design A | Design B |
|---|---|---|
| Copper loss $(kJ)$ | 85.439 | 47.22 |
| Iron loss $(kJ)$ | 234.88 | 415.9 |
| Efficiency at rated point $(\%)$ | 94.53 | 92.65 |

To make the aforementioned results more clear, the copper and iron losses are compared for both designs over the first 6 high energy points in the NEDC cycle. The results are listed in Table 11. As it is clear, in the majority of the operating points, the obtained efficiencies with "Design A" are higher.

### 3.5. FE Model Definition

Regarding to the intrinsic 3D structure of AFPM machines, 2D FEA on the machine average radius may not offer an accurate results [13]. Therefore, a 3D FEA should be performed and actual 3D structure of the machine and its 3D flux behaviour must be taken into account. Geometry complexity, nonlinear behaviour of the used materials, and electromagnetic field saturation in the machine different parts can be regarded by FEA. Considering the periodicity and axial symmetry, modelling of only one magnet, one stator stack

and 1/2 of a rotor back-iron is enough. It can be done by proper boundary conditions definition as illustrated in Figure 6.

***Table 11.*** *Energy loss component and efficiency comparison at 12 representative points for two designs*

| Speed (rad/s) | Torque (Nm) | Energy (kJ) | Design A | | |
|---|---|---|---|---|---|
| | | | $W_{cu}$ (kJ) | $W_{fe}$ (kJ) | $\eta$ (%) |
| 106.45 | 92.46 | 1445.5 | 20.08 | 20.83 | 96.16 |
| 214.72 | 77.39 | 1319.8 | 8.33 | 36.37 | 95.61 |
| 350.38 | 79.54 | 1316.3 | 6.23 | 50.85 | 94.74 |
| 60.07 | 149.41 | 852 | 34.19 | 5.62 | 94.66 |
| 216 | 139.6 | 554.5 | 6.28 | 8.5 | 96.36 |
| 325.78 | 37.12 | 423.2 | 0.97 | 33.12 | 91.35 |
| Speed (rad/s) | Torque (Nm) | Energy (kJ) | Design B | | |
| | | | $W_{cu}$ (kJ) | $W_{fe}$ (kJ) | $\eta$ (%) |
| 106.45 | 92.46 | 1445.5 | 11.33 | 36.87 | 95.53 |
| 214.72 | 77.39 | 1319.8 | 4.4 | 64.4 | 93.79 |
| 350.38 | 79.54 | 1316.3 | 2.92 | 90.1 | 92.19 |
| 60.07 | 149.41 | 852 | 19.59 | 9.95 | 95.62 |
| 216 | 139.6 | 554.5 | 3.3 | 15.06 | 95.65 |
| 325.78 | 37.12 | 423.2 | 0.466 | 58.68 | 86.33 |

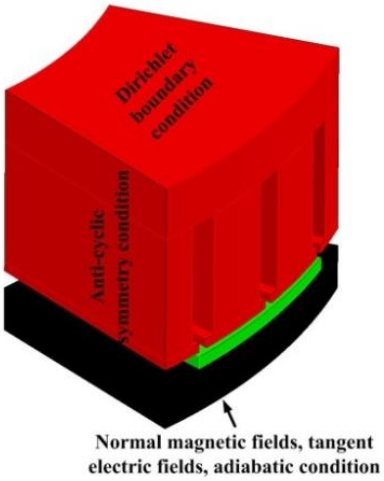


***Figure 6.*** *Model reduction in FEA*

To assess the effectiveness and accuracy of the analytical design, the machine is designed using quasi-3D approach and verified by 3D-FEA at rated operating point. Several obtained results are given in Table 12. As is obvious, there is a compromise between the quasi-3D approach and 3D-FEA. Therefore, the design data obtained by 3D-FEA is reliable enough to estimate the machine performance.

***Table 12.*** *Comparison of quasi-3d approach and 3D-FEA*

| Parameter | Quasi-3D | 3D-FEA |
|---|---|---|
| Maximum flux density in the air-gap ($T$) | 0.816 | 0.814 |
| Maximum flux density in the teeth ($T$) | 1.63 | 1.6 |
| Maximum flux density in the yoke ($T$) | 1.32 | 1.28 |
| Line-to line back-EMF (V) | 248.2 | 245 |

| | | |
|---|---|---|
| Iron loss (*W*) | 196.37 | 220.3 |
| Efficiency (%) | 95.35 | 95.28 |

## 4. CONCLUSION

In this paper, a design optimization technique based on the representative points and quasi-3D approach has been presented to improve the efficiency of an AFPM electric vehicle traction machine over a predefined driving cycle. Hundreds of operating points in a driving cycle are represented by several points and optimization is carried out against this limited number of points instead of all points. Therefore, the required time for the design optimization is significantly reduced. It has also been concluded that an optimal design data may not be achieved with a design optimized against the rated point for the machines used in EV applications. The design technique is verified by 3D-FEA.

## CONFLICTS OF INTEREST

No conflict of interest was declared by the authors.

## REFERENCES

[1] Onori, S., Serrao, L., Rizzoni, G., "Hybrid Electric Vehicles Energy Management Strategies", Springer, (2016).

[2] Shokri, M., Behjat, V., Rostami, N., "A Wind System Based on FEA of an Axial Flux Permanent Magnet Generator and Modular Multilevel Inverter", Gazi University Journal of Science, 30(2): 149-158, (2017).

[3] Lin, Y. S., Hu, K. W., Yeh, T. H., Liaw, Chang-M., "An Electric-Vehicle IPMSM Drive With Interleaved Front-End DC/DC Converter", IEEE Transactions on Vehicular Technology, 65(6): 4493-4504, (2016).

[4] Min, M. J., Jae, P. G., Hyeok, S. S., Woo, K. D., Yong, J. S., "Design Characteristics of IPMSM With Wide Constant Power Speed Range for EV Traction", IEEE Transactions on Magnetics, 53(6): 1-4, (2017).

[5] Dongjae, K., Hongsik, H., Sungwoo, B., Cheewoo, L., "Analysis and Design of a Double-Stator Flux-Switching Permanent Magnet Machine Using Ferrite Magnet in Hybrid Electric Vehicles", IEEE Transactions on Magnetics , 52(7): 1-4, (2016).

[6] Abdel-Khalik, A. S., Ahmed, S., Massoud, A. M., "A Six-Phase 24-Slot/10-Pole Permanent-Magnet Machine With Low Space Harmonics for Electric Vehicle Applications", IEEE Transactions on Magnetics, 52(6): 1-10, (2016).

[7] Zhu, Z. Q., and Howe, D., "Electrical Machines and Drives for Electric, Hybrid, and Fuel Cell Vehicles", Proceedings of the IEEE, 95(4): 746-765, (2007).

[8] Chau, K. T., Chan, C. C., Liu, C., "Overview of permanent-magnet brushless drives for electric and hybrid electric vehicles", IEEE Transactions on Industrial Electronics, 55(6): 2246-2257, (2008).

[9] Chai, F., Xia, J., Guo, B., Cheng, S., and Zhang, J., "Double-stator permanent magnet synchronous in-wheel motor for hybrid electric drive system", IEEE Transactions in Magnetics, 45(1): 1-5, (2009).

[10] Parviainen, A., Niemela, M., and Pyrhonen, J., "Modeling axial flux permanent-magnet machines", IEEE Transactions on Industrial Applications, 40(5): 1333-1340, (2004).

[11] Parviainen, A., "Design of Axial Flux Permanent-Magnet Low-Speed Machines and Performance Comparison between Radial-Flux and Axial-Flux Machines", PhD Thesis, Lappeenranta University of Technology, Lappeenranta, Finland, (2005).

[12] Rostami, N., Feyzi, M. R., Pyrhönen, J., Parviainen, A., and Behjat, V., "Genetic Algorithm Approach for Improved Design of a Variable Speed Axial-Flux Permanent-Magnet Synchronous Generator", IEEE Transactions on Magnetics, 48(12): 4860-4865, (2012).

[13] Rostami, N., and Rostami, M., "Analytical Design of AFPM Machines with Cylindrically Shaped Magnets using Quasi-3D Method", COMPEL - The International Journal for Computation and Mathematics in Electrical and Electronic Engineering, 36(4): 1168-1183, (2017).

[14] Shokri, M., Rostami, N., Behjat, V., Pyrhönen, J., and Rostami, M., "Comparison of Performance Characteristics of Axial-Flux Permanent-Magnet Synchronous Machine with Different Magnet Shapes", IEEE Transactions on Magnetics, 51(12): 1-6, (2015).

[15] Ju Hyung Kim, Yingjie Li, Bulent Sarlioglu, "Novel Six-Slot Four-Pole Axial Flux-Switching Permanent Magnet Machine for Electric Vehicle", IEEE Transactions on Transportation Electrification, 3(1): 108-117, (2017).

[16] Lehr, M., Reis, K., and Binder, A., "Comparison of axial flux and radial flux machines for the use in wheel hub drives", e & i Elektrotechnik und Informationstechnik, 132(1): 25-32, (2015).

[17] Lok, C.L., Vengadaesvaran, B., and Ramesh, S., "Implementation of hybrid pattern search–genetic algorithm into optimizing axial-flux permanent magnet coreless generator (AFPMG)", Electrical Engineering, 99(2): 751-761, (2017).

[18] Darabi, A., Baghayipour, M., and Mirzahosseini, R., "An Extended Analytical Algorithm for Optimal Designing of a TORUS-type Non-slotted Axial-Flux Permanent Magnet Motor", Journal of Control, Automation and Electrical Systems, 28(6): 748-761, (2017).

[19] Johansen, P. R., Patterson, D., O'Keefe, C., and Swenson, J., "The use of an axial flux permanent magnet in-wheel direct drive in an electric bicycle", Renewable Energy, 22(1-3): 151-157, (2001).

[20] Yang, Y. P., and Shih, G. Y., "Optimal Design of an Axial-Flux Permanent-Magnet Motor for an Electric Vehicle Based on Driving Scenarios", Energies, 9(4): 285, (2016).

[21] Chen, L., Wang, J., Lazari, P., "Influence of driving cycles on traction motor design optimizations for electric vehicles", Transport Research Arena (TRA) 5th Conference, Paris, (2014).

[22] Sarigiannidis, A. G., Beniakar, M. E., Kladas, A. G., "Fast Adaptive Evolutionary PM Traction Motor Optimization Based on Electric Vehicle Drive Cycle", IEEE Transactions on Vehicular Technology, 66(7): 5762-5774, (2017).

[23] De Santiago, J., Bernhoff, H., Ekergå andrd, B., Eriksson, S., Ferhatovic, S., Waters, R., and Leijon, M., "Electrical motor drivelines in commercial all-electric vehicles: a review", IEEE Transactions on Vehicular Technology, 61(2): 475-484, (2012).

[24] S. Kreuawan, F. Gillon, and P. Brochet, "Comparative study of design approach for electric machine in traction application", International Review of Electrical Engineering, 3(3): 455–465, (2008).

[25] Sulaiman, E., Kosaka, T., and Matsui, N., "Design and Performance of 6-slot 5-pole PMFSM with Hybrid Excitation for Hybrid Electric Vehicle Applications", International Power Electronics Conference, (2010).

[26] Lazari, P., Wang, J., and Chen, L., "A computationally efficient design technique for electric vehicle traction machines", Proc. of 20th International Conference on Electrical Machines (ICEM), France, (2012).

[27] Wynen, V., Boureima, F. S., Matheys, J., Van den Bossche, P., and Van Mierlo, J., "Developing applicable driving cycle for retrofitted Plug-In Hybrid Electric Vehicles (PHEVs): environmental impact assessment", World Electric Vehicle Journal, 3(1): 147-159, (2009).